

Estimating the H I gas fractions of galaxies in the local Universe

Wei Zhang^{1*}, Cheng Li^{2,3}, Guinevere Kauffmann², Hu Zou¹, Barbara Catinella², Shiyin Shen³, Qi Guo², Ruixiang Chang³

¹ *National Astronomical Observatories, Chinese Academy of Sciences, Beijing 100012, China*

² *Max Planck Institut für Astrophysik, Karl-Schwarzschild-Strasse 1, 85748 Garching, Germany*

³ *Key Laboratory for Research in Galaxies and Cosmology, Shanghai Astronomical Observatory, Nandan Road 80, Shanghai 200030, China*

Accepted Received; in original form

ABSTRACT

We use a sample of 800 galaxies with H I mass measurements from the HyperLeda catalogue and optical photometry from the fourth data release of the Sloan Digital Sky Survey to calibrate a new photometric estimator of the H I-to-stellar mass ratio for nearby galaxies. Our estimator, which is motivated by the Kennicutt-Schmidt star formation law, is $\log_{10}(G_{HI}/S) = -1.73238(g-r) + 0.215182\mu_i - 4.08451$, where μ_i is the i -band surface brightness and $g-r$ is the optical colour estimated from the g - and r -band Petrosian apparent magnitudes. This estimator has a scatter of $\sigma = 0.31$ dex in $\log(G_{HI}/S)$, compared to $\sigma \sim 0.4$ dex for previous estimators that were based on colour alone. We investigate whether the residuals in our estimate of $\log(G_{HI}/S)$ depend in a systematic way on a variety of different galaxy properties. We find no effect as a function of stellar mass or 4000 Å break strength, but there is a systematic effect as a function of the concentration index of the light. We then apply our estimator to a sample of 10^5 emission-line galaxies in the SDSS DR4 and derive an estimate of the H I mass function, which is in excellent agreement with recent results from H I blind surveys. Finally, we re-examine the well-known relation between gas-phase metallicity and stellar mass and ask whether there is a dependence on H I-to-stellar mass ratio, as predicted by chemical evolution models. We do find that gas-poor galaxies are more metal rich at fixed stellar mass. We compare our results with the semi-analytic models of De Lucia & Blaizot, which include supernova feedback, as well as the cosmological infall of gas.

Key words: galaxies: clusters: general – galaxies: distances and redshifts – cosmology: theory – dark matter – large-scale structure of Universe.

1 INTRODUCTION

The standard model of galaxy formation posits that galaxies form when gas cools, condenses and forms stars at the centres of dark matter halos. In recent years, there has been an explosion of ground- and space-based surveys that have allowed astronomers to obtain imaging and spectroscopy for samples of many thousands of galaxies in the local Universe and at high redshifts. The vast majority of these surveys have probed the rest-frame optical, ultraviolet or infrared regions of the spectral energy distributions of the galaxies, and have thus provided important constraints on the properties of the *stars* in these systems. Thanks to these surveys,

we have learned a huge amount about how the stellar masses and star formation rates of galaxies evolve with time. However, if we are to understand how galaxies form, we also need to understand how gas is accreted by galaxies and the efficiency with which that gas is converted into stars.

Our understanding of the cold gas content of galaxies lags considerably behind our understanding of their stellar populations. In the nearby Universe, new large surveys such as The Arecibo Legacy Fast ALFA (ALFALFA) Survey of H I, which will detect 25,000 extragalactic H I line sources out to $z \sim 0.06$ using 305m telescope and seven-beam Arecibo L-band Feed Array (ALFA) (Giovanelli et al. 2005), will do much to redress the balance, but our poor knowledge of the atomic gas content of galaxies at high redshifts is likely to persist for many more years. For this reason, there have been

* E-mail: xtwfn@bao.ac.cn

several recent attempts to calibrate colours or emission line equivalent widths as proxies for the gas-to-stellar mass ratio.

Tremonti et al. (2004) converted star formation surface densities (estimated from attenuation-corrected $H\alpha$ luminosities) to surface gas mass densities Σ_{gas} , by inverting the composite Schmidt law of Kennicutt (1998). These indirect gas mass estimates were used (in conjunction with true gas measurements for a minority of the galaxies) to argue that the observed correlation between stellar mass and gas-phase metallicity could not be explained within the context of a closed-box chemical evolution model. The same technique has been applied to high redshift galaxies by Erb et al. (2006) to interpret the redshift evolution in the mass-metallicity relation, and by Bouché et al. (2007) to argue that high redshift galaxies lie on a “universal” star formation relation. Needless to say, the conclusions reached in these papers are only valid if the same Kennicutt-Schmidt law applies at high redshifts.

Because the $H\alpha$ line is not accessible in high redshift galaxies without near-infrared spectra, there have also been attempts to calibrate gas-to-stellar mass ratios using optical or optical-infrared colours. The $H\text{ I}$ gas-to-stellar mass ratio, G_{HI}/S , has been found to correlate with optical (e.g. $u - r$) and optical-NIR (e.g. $u - K$) colours with a typical scatter of ~ 0.4 dex (Kannappan 2004, hereafter K04). Since the stellar mass of a galaxy can also be estimated from its optical/NIR flux if its redshift is known (see for example Bell et al. 2003, hereafter B03), these correlations provide a way of estimating gas masses for large samples of galaxies where only photometry is available. Although such gas fraction estimates have large errors for individual galaxies, they may still be useful for statistical studies.

In this paper we extend the analysis of K04 by examining the correlation of G_{HI}/S with additional galaxy properties, in the hope of finding an estimator of $H\text{ I}$ mass with less scatter. We first demonstrate that we reproduce the result of K04 if we use the same G_{HI}/S estimator and the same sample selection criteria as in K04. We then extend the analysis by using a larger calibrating sample of galaxies with both photometry and $H\text{ I}$ masses, and we examine the correlations between G_{HI}/S and a large variety of parameters. In particular, we show that if we combine the observed colour with an estimate of the surface brightness of the galaxy, we can reduce the scatter in our estimates of G_{HI}/S by a substantial factor. Finally, we apply our best estimator to a large sample of star-forming galaxies selected from the SDSS DR4. We show that we recover the $H\text{ I}$ mass function as estimated from the most recent blind $H\text{ I}$ survey data. We also re-examine the mass-metallicity relation of Tremonti et al. (2004) and show that there are strong residuals in this relation as a function of G_{HI}/S .

2 DATA

We use the Max Planck Institute for Astrophysics / Johns Hopkins University (MPA/JHU) SDSS DR4 database¹ as our parent sample. The sample comprises $\sim 4 \times 10^5$ objects that have been spectroscopically confirmed as galax-

ies and have data publically available in the SDSS DR4 (Adelman-McCarthy et al. 2006). Details can be found in Kauffmann et al. (2003) and Brinchmann et al. (2004). We also make use of data from the HyperLeda homogenized $H\text{ I}$ catalogue (Paturel et al. 2003) and from the 2MASS all-sky extended source catalogue (XSC; Jarrett et al. 2000).

In order to make comparisons with K04, we first construct a sample of 721 galaxies (**Sample I**) from cross-matching the parent SDSS sample, the 2MASS XSC and the HyperLeda $H\text{ I}$ catalogue using the same selection criteria as in K04. The galaxies are required to have positions matched to HyperLeda objects within $6''$ (as in K04) and to 2MASS XSC objects within $3''$ (as in Blanton et al. (2005)). Following K04, the galaxies are also restricted to lie in the redshift range of $z < 0.1$, $r < 17.77$ and have $K < 15$, as well as reliable redshifts and magnitudes based on data flags and errors (magnitude errors < 0.3 in K , < 0.4 in $H\text{ I}$, and < 0.15 in u , g and r). Here u , g and r are the SDSS Petrosian apparent magnitudes, and K is the 2MASS K -band extrapolated total magnitude.

Our second sample (**Sample II**) consists of 800 galaxies from the cross-match of the SDSS DR4 and HyperLeda $H\text{ I}$ data. The selection criteria are the same as above, except that the 2MASS-related criteria are not required here. In addition, we have visually examined the r -band image of each galaxy and dropped those galaxies that have companion galaxies within 200 arcseconds², to avoid mis-estimating the $H\text{ I}$ mass of the main galaxy. This sample will be used to derive our best estimator of the $H\text{ I}$ mass fraction. We note that the median redshift of the galaxies in both **Sample I** and **Sample II** is very low (~ 0.014 ; see Figure 5 below).

Our third sample (**Sample III**) is based on SDSS DR4. Because the calibration sample (**Sample II**) is limited at $z < 0.1$, we apply the same redshift cut to the DR4 sample. We also apply the same magnitude cuts to both samples ($r < 17.77$). Finally, a galaxy is only included in **Sample III** if there is a significant detection of the $H\alpha$ emission line in its optical spectrum, that is, if $EW(H\alpha) > 3\sigma$. Here $EW(H\alpha)$ is the equivalent width of the $H\alpha$ emission line and σ is its error. Both quantities are taken from the MPA/JHU database. This gives rise to a sample of 157,662 galaxies. We will use this sample to estimate the $H\text{ I}$ mass function and compare it to the results from real $H\text{ I}$ surveys (§ 4.1). We note that more than 99% of galaxies in **Sample II** show $EW(H\alpha) > 3\sigma$.

Finally we construct a fourth sample (**Sample IV**), which is also based on SDSS DR4, and consists of 64,305 star-forming galaxies with $r < 17.77$ and $z < 0.1$, high S/N emission lines ($S/N > 3$ for all the four emission lines on BPT (Baldwin-Phillips-Terlevich) diagram, see Brinchmann et al. 2004 for details.) and reliable estimates of oxygen abundances (magnitude errors < 0.15 in the five SDSS photometric bands; metallicities in the range of $7.5 < 12 + \log(O/H) < 9.5$). We use this sample to study whether the relation between stellar mass and gas-phase metallicity depends on the amount of gas in the galaxy (§ 4.2).

Throughout this paper we use stellar masses estimated

¹ <http://www.mpa-garching.mpg.de/SDSS/DR4/>

² We have also selected a smaller sample consisting of 129 galaxies that have no companions within 10 arcminutes and found no significant change in the resulting $H\text{ I}$ gas estimator.

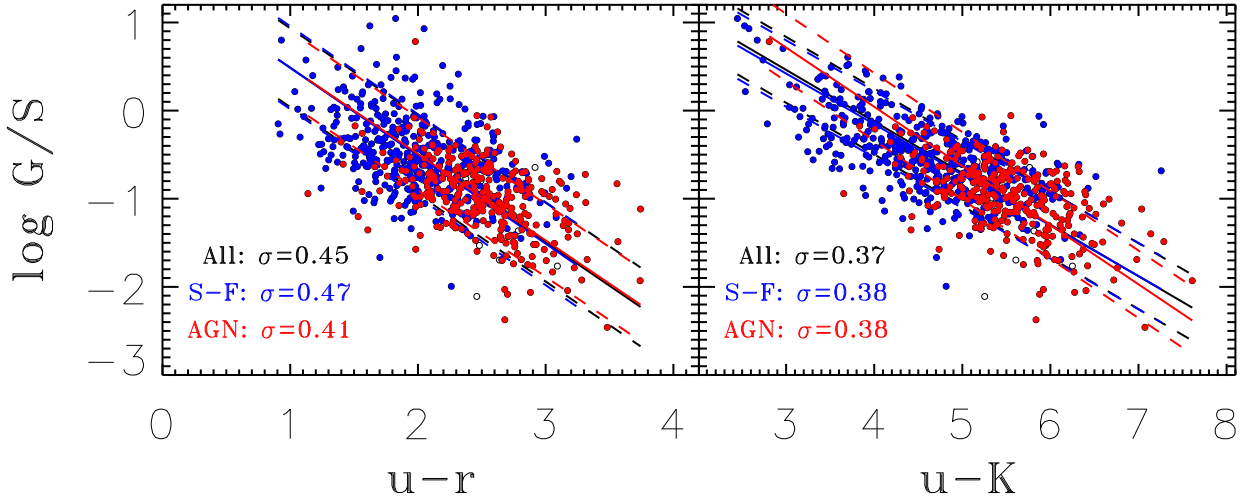


Figure 1. Correlation of the atomic gas-to-stellar mass ratio, G/S , with $u-r$ (left panel) and $u-K$ (right panel) colours, for 721 galaxies in **Sample I** that are selected from the main sample of SDSS DR4 and also have data from HyperLeda and 2MASS. Galaxies are plotted in red dots if they are classified as AGN, blue dots if they are classified as high S/N star-forming galaxies, and open circles if they are unclassified by Brinchmann et al. (2004). Gas masses are derived from H I fluxes with a helium correction factor of 1.4 as in Kannappan (2004), and stellar masses are derived from K -band fluxes using stellar mass-to-light (M/L) ratios estimated from $g-r$ colours as in Bell et al. (2003). The three lines are the best-fitting linear relation (solid) and the 1σ variance (dashed), which are shown in red for the AGN, in blue for the high S/N star-forming galaxies, and in black for the galaxies as a whole. The best-fit relations for the whole sample are $\log(G/S) = 1.48 - 0.99(u-r)$ and $\log(G/S) = 2.19 - 0.58(u-K)$ with $\sigma = 0.45$ and 0.37 dex, in good agreement with Kannappan (2004) who found $\log(G/S) = 1.46 - 1.06(u-r)$ and $\log(G/S) = 1.87 - 0.56(u-K)$ with $\sigma = 0.42$ and 0.37 dex.

from the i -band luminosity and $g-r$ colour using the formula provided in B03, that is, $\log(M_*/L_i) = -0.222 + 0.864(g-r)$. The surface brightness used here is defined as $\mu_i = m_i + 2.5 \log(2\pi R_{50}^2)$, where m_i is the apparent Petrosian i -band magnitude and R_{50} is the radius (in units of arcsecond) enclosing 50% of the total Petrosian i -band flux. The stellar surface mass density is given by $\log(\mu_*) = \log(M_*) - \log(2\pi R_{50}^2)$, where M_* is the stellar mass and R_{50} is defined in the same way as above but in units of kpc. The SDSS apparent magnitudes are corrected for foreground extinction and are k -corrected to their $z = 0$ value using the `kcorrect v4.1.4` code of Blanton et al. (2003). The 2MASS K -band magnitude is k -corrected using $k(z) = -2.1z$ (see B03). Other parameters such as star formation rate (SFR), oxygen abundance, and emission line fluxes are taken from the MPA/JHU database. The reader is referred to Brinchmann et al. (2004), Kauffmann et al. (2003) and Tremonti et al. (2004) for detailed description of how these quantities are derived. We use the *total* SFR for which the aperture bias is corrected using resolved imaging. Throughout this paper we assume a cosmological model with $\Omega_0 = 0.3$, $\Lambda_0 = 0.7$, and $H_0 = 70 \text{ km s}^{-1} \text{ Mpc}^{-1}$.

3 ESTIMATING GAS MASSES

3.1 Correlations of G_{HI}/S with galaxy properties

In Fig. 1 we plot the correlation of the atomic gas-to-stellar mass ratio, G/S , with $u-r$ (left panel) and $u-K$ (right panel) colours for the 721 galaxies in **Sample I**. The atomic gas masses and the stellar masses plotted here are estimated in exactly the same way as in K04. Briefly, gas masses are de-

rived from H I fluxes with a helium correction factor of 1.4, while stellar masses are from K -band fluxes using stellar mass-to-light (M/L) ratios estimated from $g-r$ colours as in B03. The only difference from the analysis of K04 is the fact that our sample is based on a later SDSS data release. Using a sample of 346 galaxies constructed from cross-matching the SDSS DR2, the 2MASS XSC and the HyperLeda H I catalogue, K04 found $\log(G/S) = 1.46 - 1.06(u-r)$ and $\log(G/S) = 1.87 - 0.56(u-K)$ with 1σ variance $\sigma = 0.42$ and 0.37 dex. As can be seen from Figure 1, the result of K04 is well reproduced, both in the overall amplitude and slope of the mean correlations, and in the scatter about the mean. We also divide our sample into star-forming galaxies and AGN using the standard BPT classification diagram (see Kauffmann et al. 2003; Brinchmann et al. 2004, for details) and plot these two classes using different colour codings. As can be seen, AGN and star-forming galaxies do not show significant difference in their correlation between gas fraction and colour. We therefore do not remove AGN from any of our samples, with the exception of sample IV, because we cannot obtain accurate gas-phase metallicity measurements for AGN.

We then examine the correlations between G_{HI}/S and a variety of physical quantities, in the hope of finding a even better estimator for the gas fraction. It has long been established that the fraction of atomic gas correlates with a variety of galaxy properties. It would certainly not be surprising to find that a higher gas content is associated with galaxies with lower stellar masses, bluer colours, lower surface brightnesses, disk-dominated morphologies and spectral types indicative of the presence of a young stellar population. In our calibrating sample, G_{HI}/S exhibits the *tightest* correlations with colour, surface brightness and stellar sur-

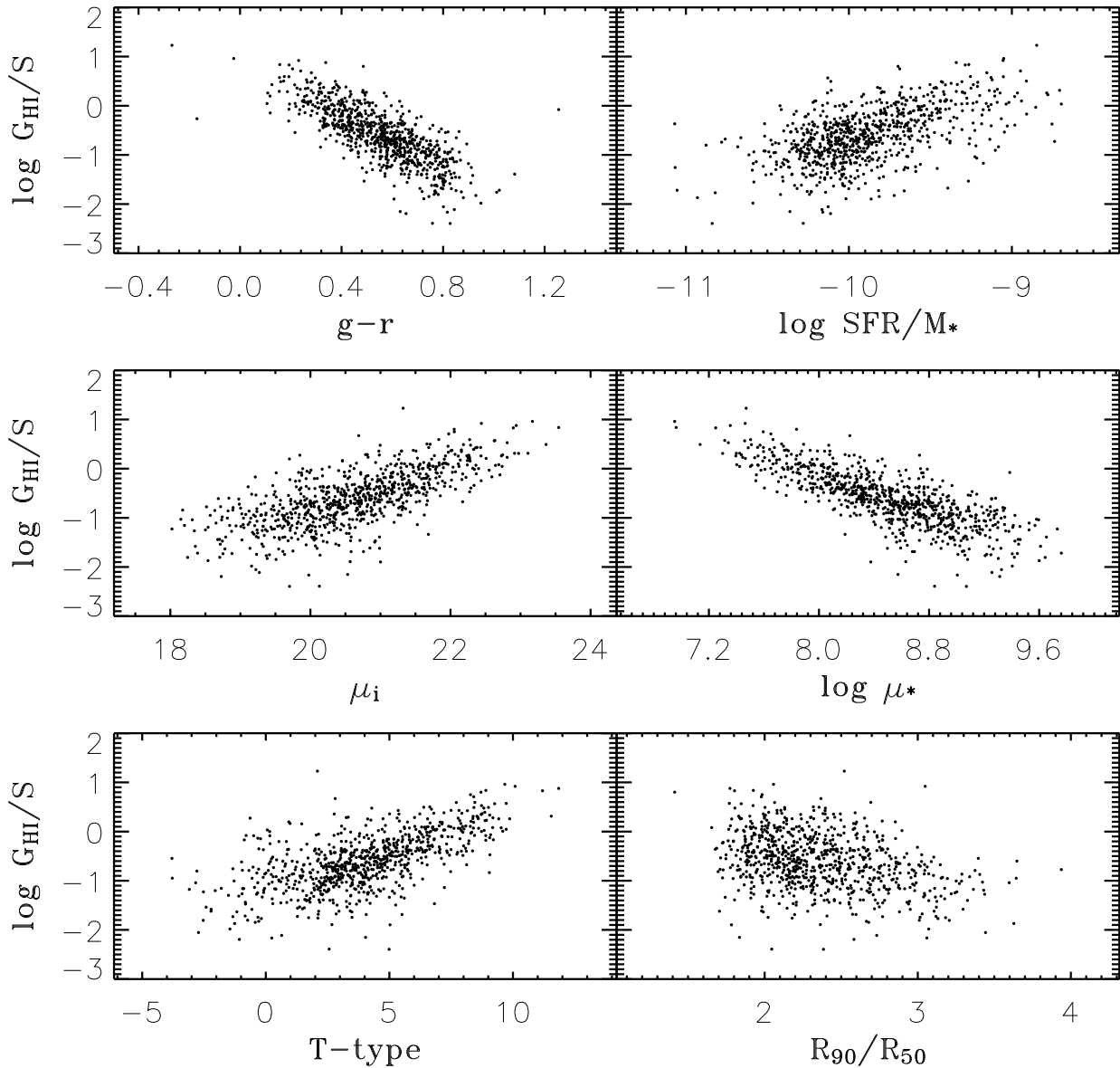


Figure 2. Correlation of the atomic gas-to-stellar mass ratio, G/S , with $g-r$ colour (top left), aperture corrected specific star formation rate from Brinchmann et al. (2004) (top right), i -band surface brightness (middle left), stellar surface mass density (middle right), T-type (bottom left, see text for more explanation), and concentration index (bottom right) for 800 galaxies in **Sample II**

face mass density, with a typical scatter of ~ 0.4 dex (see Fig. 2). Interestingly, we find that the correlation between G_{HI}/S and i -band surface brightness or surface stellar mass density is much tighter than the correlation between G_{HI}/S and concentration index, which provides a good measure of the bulge-to-disk ratio of the galaxy (Gadotti 2009).

We have also examined another indicator of morphology, T-type (de Vaucouleurs et al. 1991). We estimate this quantity using a back propagation neural network (BPNN). The basic methodology we employ (number of layers and neurons, the transfer function, the training algorithm etc) are exactly the same as described in Ball et al. (2004). The

training and test samples are drawn from the RC3 and consist of 4393 galaxies with imaging data from the SDSS DR4. We follow Fukugita et al. (2007) and use 29 photometric parameters, which are available from SDSS, as the input for the BPNN. The inner structure of the network is adjusted iteratively until an optimally trained network that links T and the available set of photometric parameters is obtained. The network is then applied to the galaxies in our sample with no T measurement. As can be seen from the figure, the correlation of G_{HI}/S and T-type is also weaker than the correlation with surface mass density or surface brightness.

We find that G_{HI}/S correlates very strongly with

galaxy colour and reasonably strongly with specific star formation rate (corrected for aperture effects as described in Brinchmann et al. 2004). We also find correlations with other quantities, but since all of them exhibit considerably more scatter, we do not show them here.

3.2 Deriving new G_{HI}/S estimators

In this paper, we will only concern ourselves with our two strongest correlations: i.e the correlation between G_{HI}/S and colour or specific star formation rate and the correlation between G_{HI}/S and surface brightness or stellar surface mass density. How can these correlations be understood? Let us consider the Kennicutt-Schmidt law of star formation (Schmidt 1963; Kennicutt 1998) in which the surface density of star formation rate scales with the surface density of total (atomic+molecular) cold gas as an increasing power law,

$$\Sigma_{SFR} \propto \Sigma_{gas}^n, \quad (1)$$

with a slope of $n \approx 1.4$. If the two surface densities are estimated over the same radius, one can easily rewrite the Kennicutt-Schmidt law as follows:

$$SFR/M_* \propto (G/S)^n \mu_*^{n-1}, \quad (2)$$

where $G/S \equiv M_{gas}/M_*$, and M_{gas} and M_* are the total mass of cold gas and stars. It is thus natural to expect the gas mass-to-stellar mass ratio to correlate with these properties, just as shown in Figure 2. More interestingly, the above equation implies that there exists a plane of correlations, similar to the fundamental plane of early-type galaxies, involving the following three variables: the gas-to-stellar mass ratio (G/S), the specific star formation rate (SFR/M_*) and the surface stellar mass density (μ_*). This plane can be defined by

$$\log G/S = \log M_{gas}/M_* = a \log \mu_* + b \log SFR/M_* + c, \quad (3)$$

where the coefficients a , b , and c can be determined by minimizing the residuals from the plane. If the gas content parameter G/S that enters this plane scales linearly with the observed H I-to stellar mass ratio (we admit that this may well be an over-simplification of the true situation), then $\log G_{HI}/S$ can also be expressed as a linear combination of the logarithm of the stellar surface mass density and the logarithm of the specific star formation rate.

Our best-fit relation between G_{HI}/S and the linear combination of μ_* and SFR/M_* (from **Sample II**) is shown in the far-right panel of Figure 3. The galaxies are plotted as black dots, and the best-fit relation is shown as a solid line. The 1σ scatter around the relation is 0.33 dex, which is significantly smaller than the scatter in the relation between $\log G_{HI}/S$ and stellar surface mass density or the relation between $\log G_{HI}/S$ and specific star formation rate.

This relation is also tighter than the correlations of G_{HI}/S with all the other galaxy properties we have investigated. Thus, this relation can serve as a better estimator of H I-to-stellar mass ratio, compared to those derived using a single parameter.

We note that the correlation between colour and G_{HI}/S shown in Figure 2 is actually somewhat *tighter* than the correlation between SFR/M_* and G_{HI}/S . One reason for

this may be that the Brinchmann et al (2004) aperture corrections are not accurate. As shown in Brinchmann et al. (2004) (see their Fig. 14), for $\log(SFR/M_*) > -10.5$, the 2σ uncertainties on the aperture-corrected log SFRs are larger by ~ 0.3 dex than for log SFR measured inside the fibre because the aperture corrections are significantly more uncertain than the SFR estimates from the spectra. The errors will be even larger for the galaxies in our sample, because the median redshift is much lower and the total star formation rates are derived almost entirely from the photometry, not from the emission lines measured in the spectra.

In addition, we find the correlation between G_{HI}/S and surface brightness is just as tight as the correlation between G_{HI}/S and stellar surface mass density, so there is no real value in working with the Brinchmann et al. (2004) star formation rate estimates, rather than with directly measured colours. For our purposes, this is in fact quite encouraging, because it suggests that one can get a reasonably good prediction for the fraction of atomic gas in a galaxy from photometrically measured quantities. This is most frequently available for high redshift galaxies.

We propose that the $(g-r)$ colour and i -band surface brightness μ_i are good choices for this purpose. The correlation plane that uses the quantities $(g-r)$ and μ_* is shown in the leftmost panel in Figure 3, and the plane that uses the quantities $(g-r)$ and μ_i is shown in the central panel. The scatters in the relations are the same (0.31 dex), even smaller than the plane involving SFR/M_* and μ_* . We thus adopt the relation in the central panel,

$$\log_{10}(G_{HI}/S) = -1.73238(g-r) + 0.215182\mu_i - 4.08451, \quad (4)$$

as our final estimator of G_{HI}/S . The scatter in our new estimator represents a 20% decrease as compared in that of K04.

Before we go ahead and apply this estimator to large samples or try to extrapolate it to higher redshifts, it is important to test whether we can find any systematic effects that could bias such analyses. For example, we know that pure passive aging of stellar populations will cause the colour of a galaxy to evolve with time. It would therefore not be surprising if G_{HI}/S at a fixed value of the $g-r$ colour was to depend on redshift. In the absence of H I data for high redshift galaxies, the only way we can test for such effects is to see whether the *residuals* around our best-fit estimator are correlated with intrinsic properties of the galaxies, such as stellar mass, morphology or mean stellar age. In Figure 4 we plot the residuals of G_{HI}/S from the relation given in Eq.(4) as a function of stellar mass, concentration index and 4000 Å break strength. There is no clear tendency for the G_{HI}/S residuals to correlate with stellar mass or with 4000 Å break strength. There is a small, but significant trend in the residual as a function of the concentration index, in the sense that our estimator overpredicts the gas fraction for the least concentrated galaxies and underpredicts for the most concentrated objects. The effect is not large — ~ 0.2 dex shift in the predicted value of $\log G_{HI}/S$ from the least concentrated to the most concentrated galaxies in our sample. We do not see significant trends in the scatter in the residuals as a function of any galaxy property, suggesting that it may be possible to calibrate out such systematic trends in the future.

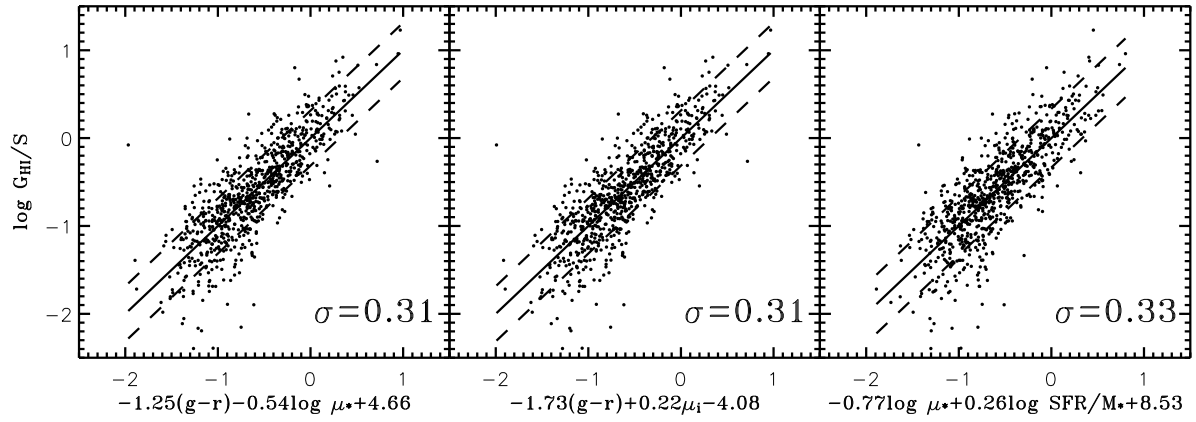


Figure 3. We plot the relations between G_{HI}/S and the linear combinations of, a) $g-r$ colour and stellar surface mass density (left), b) $g-r$ colour and i -band surface brightness (middle), and c) aperture corrected specific star formation rate from Brinchmann et al. (2004) and stellar surface mass density, that minimize the scatter.

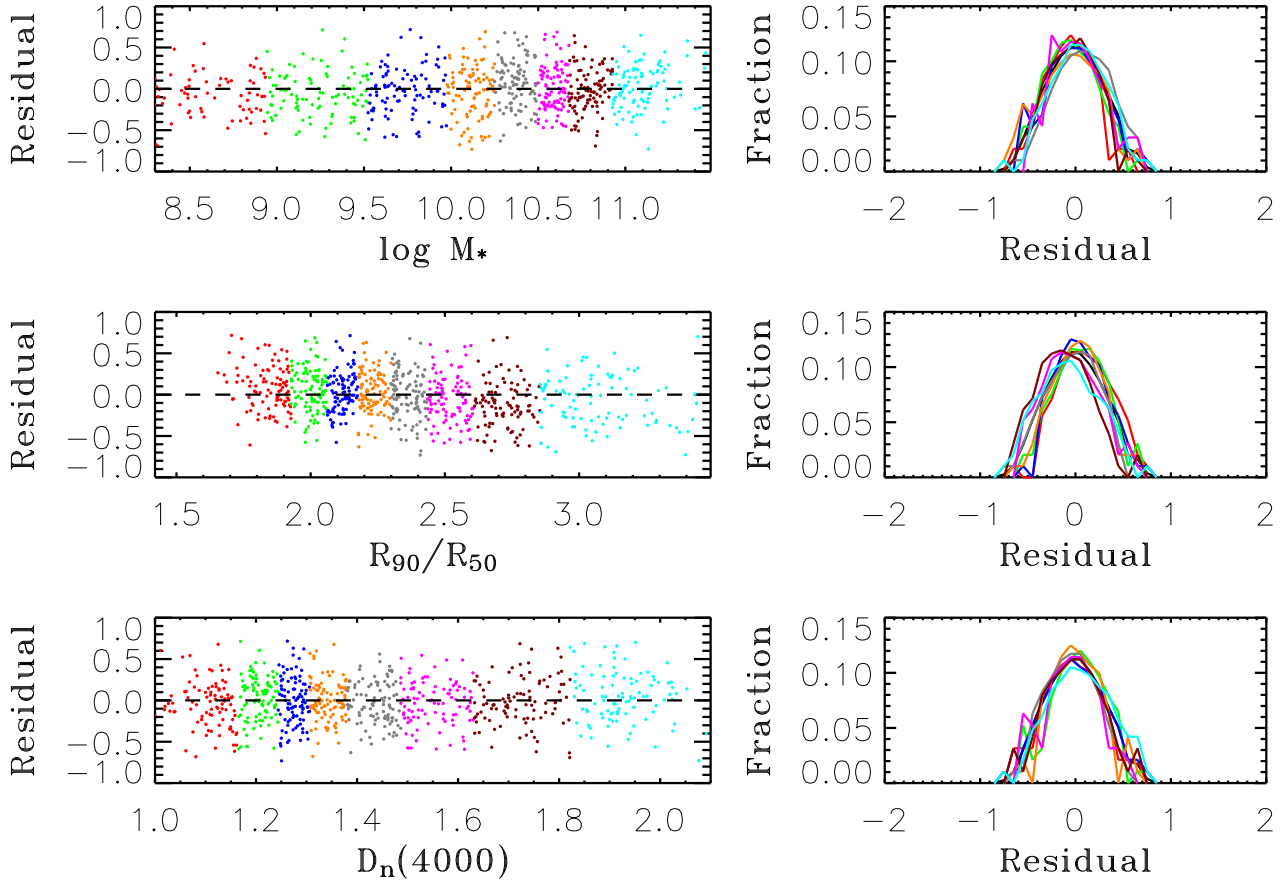


Figure 4. We plot the residual in the predicted value of G_{HI}/S from equation (4) as a function of stellar mass (top left), concentration index (middle left) and 4000 Å break strength (bottom left). We have also divided the galaxies into 8 subsamples as indicated by the coloured dots (left panels) or lines (right panels). The left panels show the residual for individual galaxies, while the right panels show the distribution of the residuals in each of the subsamples.

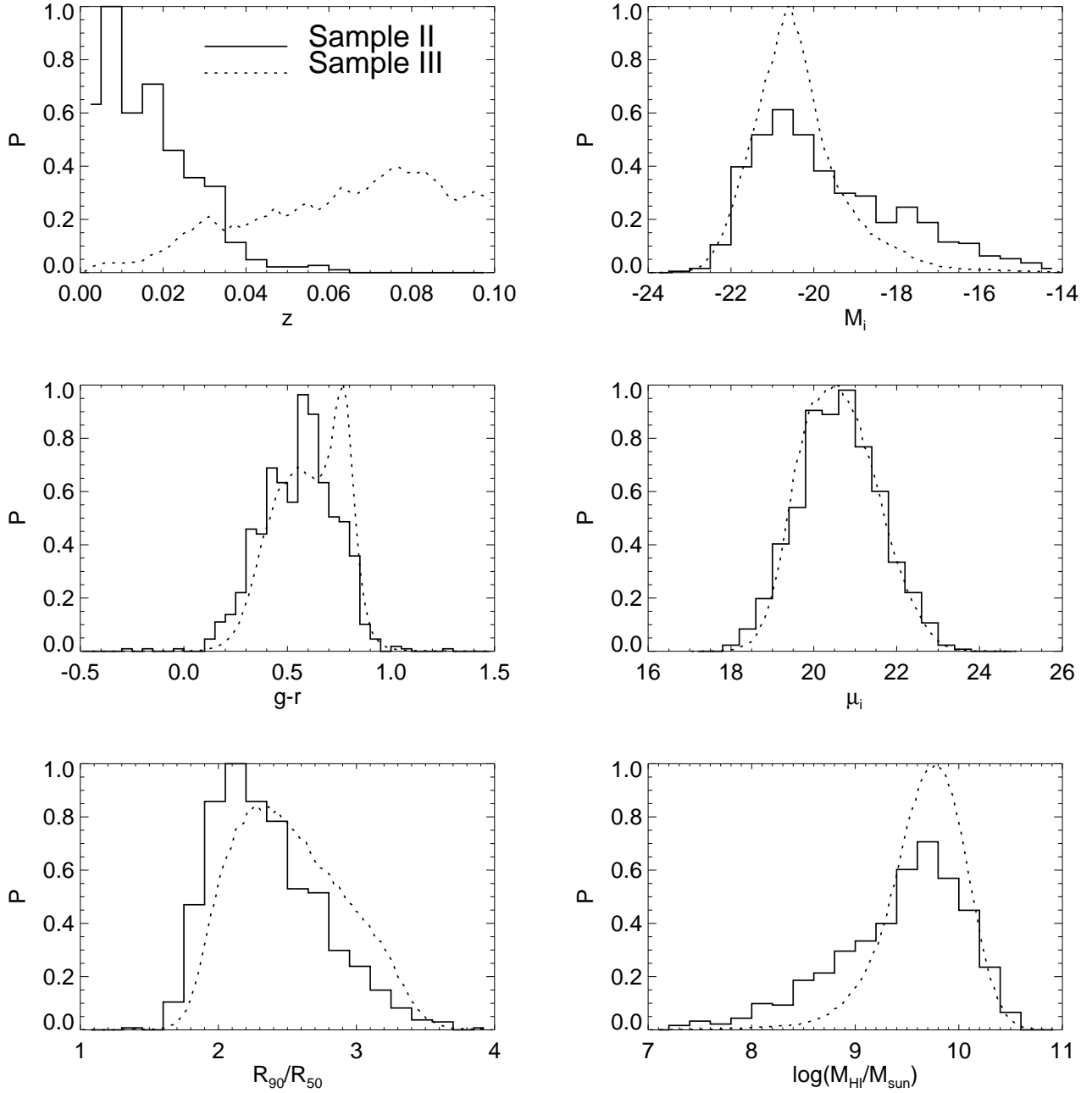


Figure 5. Distributions of redshift, i -band absolute magnitude, $g-r$ colour, i -band surface brightness, concentration parameter R_{90}/R_{50} measured in i -band, and H I gas mass, for galaxies in our calibration sample (**Sample II**, solid line) and in **Sample III** (dotted line). In each panel the maximum of the two curves is set to unity and the two curves are normalized so that they enclose the same area.

We caution that our calibrating sample is compiled from many different samples with different selection effects, and may thus be biased because it is *not* a truly representative sample of nearby galaxies. This can be seen from Figure 5 where we plot the histograms of a variety of physical properties for galaxies in **Sample II**. It will be important to re-examine these issues with larger and more homogeneous galaxy samples, as will be provided by the ALFALFA survey.

4 APPLICATIONS

We now illustrate two different applications of our G_{HI}/S indicator. We first use the colours and surface brightnesses of the galaxies in **Sample III** to estimate the H I mass function and we compare our estimate with recent results from real H I surveys. We then examine whether residuals in the relation between gas phase metallicity and stellar mass are correlated with the H I content of galaxies.

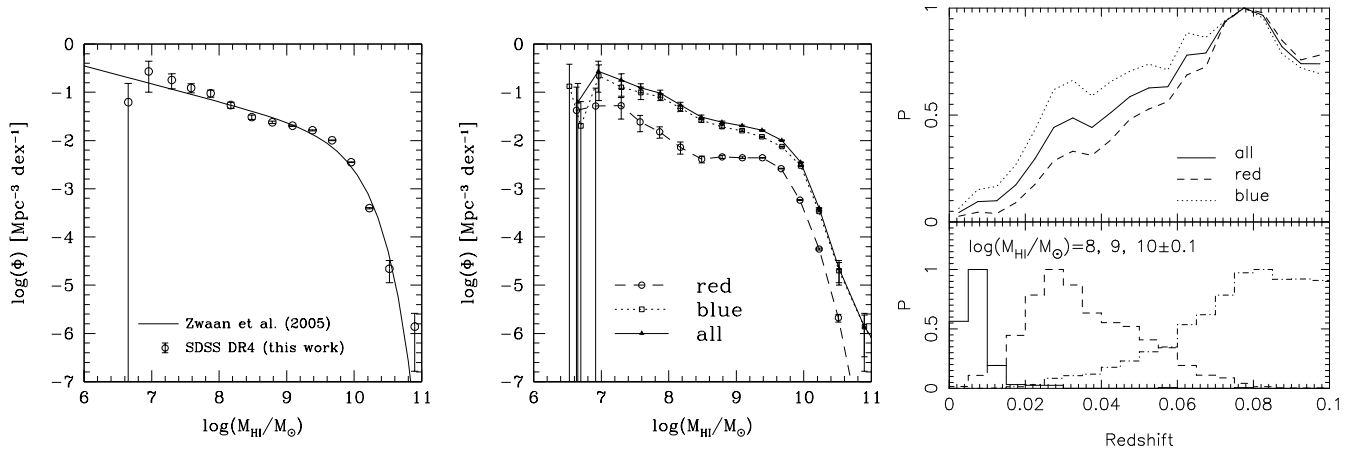


Figure 6. *Left:* H I mass function for the galaxies in the SDSS DR4 that have redshift below 0.1 and evident H α emission in their optical spectrum is plotted as symbols, compared to the result from previous study which is based on real H I observation and is plotted as line. *Center:* H I mass function is plotted for red/blue galaxies separately. The result for the full sample is repeated from the left panel. *Right:* redshift distributions for red and blue galaxies as well as for the galaxies as a whole are plotted in the upper part. The lower part shows the redshift distribution for galaxies in the full sample, but at three fixed stellar masses as indicated.

4.1 H I Mass Function

For each galaxy i in SAMPLE III we compute the quantity $z_{max,i}$, which is defined as the maximum redshift at which the galaxy would satisfy the apparent magnitude limit of the sample. k -corrections are included when calculating $z_{max,i}$ as described in Blanton et al. (2003) (see also Blanton & Roweis 2007). We do not apply evolutionary corrections, because our sample is constrained to lie at $z < 0.1$. $V_{max,i}$ is defined for each galaxy as the comoving volume of the survey out to redshift $z_{max,i}$, or 0.1 if $z_{max,i} > 0.1$. The H I mass function is thus estimated as

$$\Phi(M_{HI})\Delta M_{HI} = \sum_i (f_{sb,i} V_{max,i})^{-1}, \quad (5)$$

where $f_{sb,i}$ is the spectroscopic completeness of the survey area where the galaxy i is located and is defined as the fraction of the photometrically targeted galaxies in the area for which usable spectra were obtained. The sum in the above equation extends over all galaxies with H I mass in the range $M_{HI} \pm 0.5\Delta M_{HI}$.

Figure 6 shows the H I mass function for galaxies in Sample III. The error bars are estimated using the bootstrap resampling technique (Barrow et al. 1984). We generated 100 bootstrap samples from Sample III and computed the H I mass function for each sample. The errors are then given by the scatter of the mass function among these samples. We would like to point out that these errors are underestimated, because they account only for the uncertainties due to sampling variance, but do not include the effect of cosmic variance, systematic uncertainties in the estimates of stellar masses, and scatter in the estimates of H I mass. For comparison, we also plot in Figure 6 a recent measurement of the H I mass function by Zwaan et al. (2005), based on a complete H I-selected sample of 4315 galaxies from the HI Parkes All Sky Survey (HIPASS). HIPASS achieves 100% coverage over the southern sky and the samples used for calculating the H I mass functions lie in the redshift range $0.003 < z < 0.02$. Most other determinations of the H I mass function have been based on signif-

icantly smaller samples (Zwaan et al. 1997; Henning et al. 2000; Rosenberg & Schneider 2002; Zwaan et al. 2003), or have been based on samples containing only specific morphological types (Springob et al. 2005).

Our derived H I mass function is in excellent agreement with the Zwaan et al. (2005) result and is reasonably well fit by a single Schechter function with parameters close to those given by Zwaan et al. (2005). A comparison of our measured H I mass function with their best-fit Schechter function gives a reduced χ^2 statistic of $\chi^2/d.o.f = 24/12$. Their parameters yield slightly fewer galaxies at the low-mass end. A straightforward integration of our H I mass function gives the mean comoving H I mass density of the low-redshift Universe of $\rho_{HI} \sim 7.5 \times 10^7 h M_\odot / \text{Mpc}^3$, corresponding to a cosmological H I mass density of $\Omega_{HI} \sim 2.7 \times 10^{-4} h^{-1}$, again well consistent with Zwaan et al. (2005). In the standard concordance cosmology (e.g. Komatsu et al. 2009) this matter density corresponds to only $\sim 0.8\%$ of the baryons in the low-redshift Universe in H I gas in galaxies, compared to 3.5% in stars (Li & White 2009).

It is also interesting to compare the relative abundance of red and blue galaxies at given H I mass. We split the sample into two colour bins using the following, luminosity-dependent cut:

$$(g - r) = -0.104 - 0.042M_r. \quad (6)$$

We then compute the H I mass functions for the red and blue subsamples separately and plot them in the right-hand panel of Figure 6. The result for the full sample is also plotted. As can be seen, the H I mass function is dominated by blue galaxies at all masses.

The redshift distribution of the red/blue subsamples as well as that of the full sample is shown in the far-right panel in Figure 6. The distribution of other physical properties of the full sample is plotted in dashed lines in Figure 5. The redshift distributions show strong features which reflect large-scale structure. The structure at $z \sim 0.08$ is the well-known super cluster in SDSS, the Sloan Great Wall. Two other weaker structures are also seen at redshifts around 0.01 and 0.03. These structures are likely the reason why our H

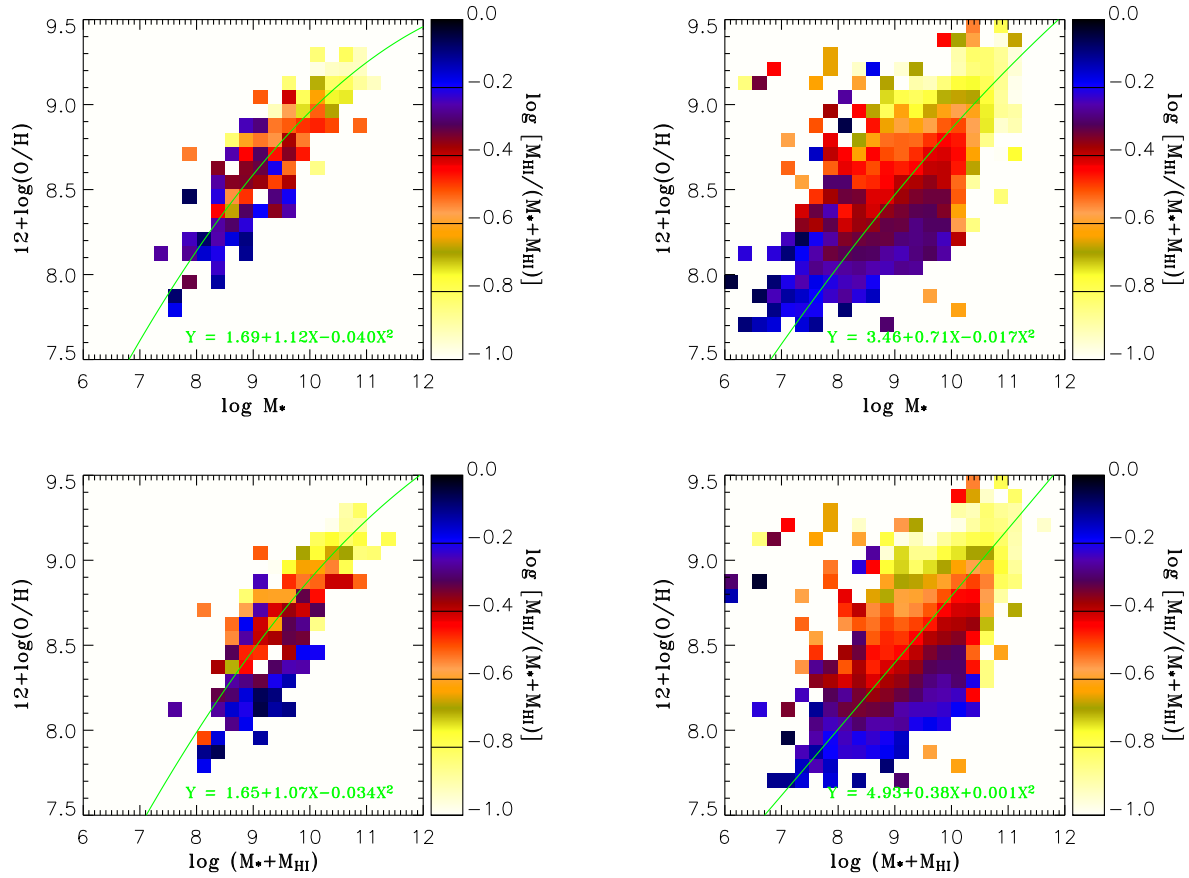


Figure 7. Correlation of metallicity with stellar mass (top) and with stellar mass plus H I gas mass (bottom). The left-hand panels show results for a sample of 800 galaxies from the HyperLeda catalogue for which the H I mass is actually measured. The right hand panels show results for 1.4×10^5 star-forming galaxies in SDSS DR4 for which the H I mass is given by our estimator based on the *i*-band surface brightness and *g* - *r* colour. Each pixel in the mass-metallicity plane has been colour-coded according to the mean H I gas fraction of the galaxies that fall in that region. The green line in each panel shows the 2nd-order polynomial function that provides the best fit to the mean relation.

I mass function shows slightly higher (but still within error bars) amplitude than that of Zwaan et al. (2005), at masses below $\sim 10^9 M_\odot$ and at those around the characteristic mass ($10^{9.8} M_\odot$). However, given the large uncertainties in our H I mass estimates and the small sample size of Zwaan et al. (2005), such discrepancies should not be overemphasised.

4.2 The Mass-Metallicity Relation

The relationship between mass and metallicity (MZR; Lequeux et al. 1979; Tremonti et al. 2004) is of particular interest in studies of galaxy formation and evolution. There is now observational (e.g. Garnett 2002; Tremonti et al. 2004) evidence that metal loss via galactic winds (Larson 1974) may be largely responsible for driving the relation. However, other processes may also be important. For example, low-mass galaxies have higher gas fractions (e.g. Boselli et al. 2002) and are hence expected to be less enriched even if they were to evolve as closed boxes. It has even been proposed that a variable IMF could also produce a mass-metallicity relation (Köppen et al. 2007).

In addition, the mass-metallicity relation has been found to depend on other properties of the galax-

ies in the sample (for example surface mass density [Tremonti et al. 2004], star formation rate as measured by ultraviolet-luminosity and surface brightness [Hoopes et al. 2007], specific star formation rate and size [Ellison et al. 2008], the presence or absence of close companions [e.g. Michel-Dansac et al. 2008], cluster membership and local density [Ellison et al. 2009] and also on large-scale environment [e.g. Cooper et al. 2008]). It would be useful to figure out which of these dependencies are primary causes of variation in the relation, and which are secondary effects. For example, if the mass-metallicity relation depends on specific star formation rate, it will naturally also depend on environment, simply because the specific star formation rates of galaxies depend strongly on density.

The gas mass fraction is the natural parameter for quantifying the degree to which a galaxy has exhausted its available fuel supply and one would expect the mass-metallicity relation to depend quite strongly on this quantity. In Figure 7, we examine the trend of gas mass fraction, defined as the ratio of H I gas mass to the sum of H I and stellar mass, with the location of galaxies in the plane of metallicity versus stellar mass (top) and metallicity versus H I mass plus stellar mass (bottom). In each case, we compare

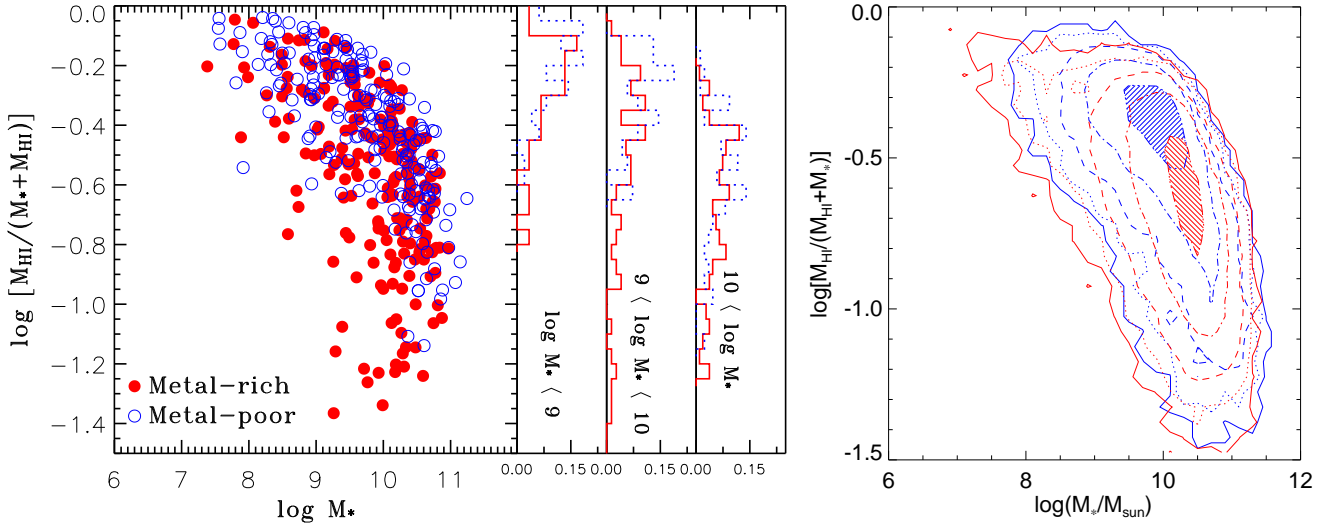


Figure 8. *Left:* H I gas mass fraction versus stellar mass relation for metal-rich (red) and metal-poor (blue) galaxies, for a small sample of galaxies that have real H I observations. The three small panels compare the histogram of H I gas fraction for metal-rich (red solid) and metal-poor (blue dashed) galaxies in three stellar mass intervals as indicated. *Right:* contours of number density of galaxies in the plane of H I gas mass fraction versus stellar mass, for a large sample of star-forming galaxies from the SDSS DR4 with H I mass estimated from photometry. Red and blue lines are for metal-rich and metal-poor galaxies respectively. The contour levels, which indicate the fraction of galaxies in the two subsamples that fall within a given region of the plane, are decreased by factors of 4 from the highest ($0.016 [0.2 \log_{10} M_{\odot}]^{-1} [0.05 \text{ dex}]^{-1}$) to the lowest ($6.25 \times 10^{-5} [0.2 \log_{10} M_{\odot}]^{-1} [0.05 \text{ dex}]^{-1}$). The region enclosed by the highest-level contour is shaded in red (blue) for the metal-rich (-poor) population.

results for our small calibrating sample with real H I masses (**Sample II**, left-hand panels) with results obtained for all high S/N star-forming galaxies (**Sample IV**, right-hand panels). As can be seen, the basic trend is very similar for the two samples. Star-forming galaxies with lower masses and metallicities have higher gas fractions.

In addition, Figure 7 shows that at fixed stellar mass, metal poor galaxies have higher H I fractions than metal-rich galaxies. This is clearly seen in Figure 8 where we plot the gas fraction—stellar mass relation for galaxies in **Sample II** and **Sample IV**. Metal-poor galaxies are plotted in blue, while metal-rich galaxies are plotted in red. In order to split our sample into two subsamples in metallicity, we determine a stellar mass-dependent cut in metallicity by fitting a 2nd order polynomial function to the stellar mass-metallicity relation shown in the top two panels of Figure 7. A galaxy located above (below) this cut is thus classified as metal-rich (-poor). As can be seen from Figure 8, metal-poor galaxies are shifted almost vertically in this diagram, towards higher H I fractions. This is true for both our calibrating sample and for the full sample of star-forming galaxies. One possible interpretation of this result, is that the scatter of metallicity at fixed stellar mass might be partially (if not totally) due to recent inflow of less enriched gas from the surrounding halo.

In order to test whether this explanation is plausible, one requires a model for the chemical enrichment of galaxies that takes into account the effect of supernova-driven winds and the infall of gas from the surrounding halo. Such models already exist. For example, De Lucia et al. (2004) implemented a model for the chemical enrichment of galaxies in a high resolution simulation of a Λ CDM universe. The transport of metals between the stars, the cold gas in galax-

ies, the hot gas in dark matter haloes and the intergalactic gas outside virialized haloes was modelled in detail. In the scheme adopted by the authors, metals are ejected outside the halo by supernovae and later reincorporated when structure collapses on larger scales. The model also followed the continued infall of cold gas onto the galaxy through merging of gas-rich satellites and through cooling from a surrounding hot gas halo. After suitable adjustments to the free parameters in the model, a good fit to the observed relations between stellar mass, gas mass and metallicity was obtained.

We now test whether these same models can reproduce the secondary trend with gas fraction that we see in our data. In Figure 9, we plot the stellar mass-gas fraction relation predicted by the semi-analytic model of De Lucia & Blaizot (2007), which incorporates the same chemical enrichment scheme as in De Lucia et al. (2004). We have selected all galaxies in the $z=0$ catalogue (available at <http://www.mpa-garching.mpg.de/millennium>) with specific star formation rates $\log_{10}(SFR/M_*) > -11$. Note that in **Sample IV** 99% galaxies have specific star formation rate above this value. As in the previous figure, the galaxies are divided into two types, “metal-poor” and “metal-rich” by defining a stellar mass-dependent cut in exactly the same way as was done for the sample of observed galaxies. As can be seen, the models do predict a displacement of the metal-poor with respect to the metal-rich subsamples that is qualitatively reminiscent of the trend seen in the real data (see also de Rossi et al. 2009, for a similar finding for Milky Way type systems in the Millennium Simulation). However, the quantitative agreement is not so good. In particular, in the simulations, the two populations are displaced more along the x-axis (i.e. in stellar mass) than along the y-axis

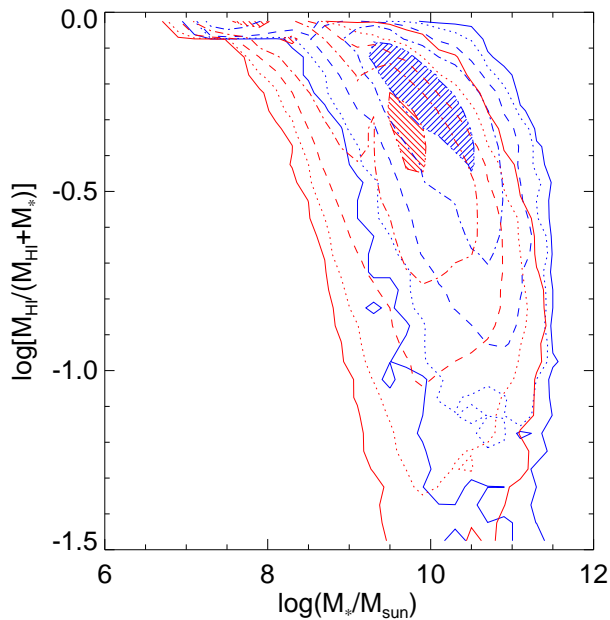


Figure 9. Gas mass fraction versus stellar mass relation for metal-rich (red) and metal-poor (blue) galaxies in the $z = 0$ semi-analytic catalogue of De Lucia & Blaizot (2007). The meaning of the colour coding and contour levels is the same as in the right-hand panel of the previous figure.

(i.e. in gas fraction), whereas the opposite is seen in the real data.

This may indicate the efficiency with which supernovae are assumed to expel gas from galaxies is too high and that the mass-metallicity trends in the real data are more driven by variations in cold gas content than in the De Lucia & Blaizot (2007) models. There is a free parameter in the models that controls the efficiency with which energy from supernova couples to the gas, and as this increases, the mass-metallicity relation steepens. Variations in gas fraction are determined by cooling and infall, which should be modeled more accurately.

One issue that we have swept under the carpet until now, is that we are assuming that the total gas content of the galaxy simply scales in proportion to the H I mass, thereby neglecting any intrinsic variations in the ratio of atomic-to-molecular gas in galaxies. If this ratio were to depend systematically on metallicity (see for example Krumholz et al. 2008), then part of the vertical displacement in H I fraction between metal-poor and metal-rich galaxies may simply be due to this effect.

5 SUMMARY

We have examined the correlation of atomic hydrogen-to-stellar mass ratio, G_{HI}/S , for a sample of 800 galaxies that have H I flux measurement from the HyperLeda catalogues and optical photometry from the SDSS DR4. We use this sample to derive a new estimator of H I mass fraction for low-redshift galaxies ($z < 0.1$). This is $\log_{10}(G_{HI}/S) = -1.73238(g - r) + 0.215182\mu_i - 4.08451$, where μ_i is the

i -band surface brightness and $(g - r)$ is the optical colour given by the g - and r -band Petrosian magnitudes. The typical scatter in the relation is 0.31 dex. We have tested whether the residuals in our G_{HI}/S estimator correlate with galaxy properties. We find no effect as a function of stellar mass or as a function of mean stellar age as measured by the 4000 Å break, but there is a small effect as a function of galaxy concentration.

We then apply this new estimator to a large sample of star-forming galaxies from the SDSS DR4 to estimate the H I mass function, and we find good agreement with determinations from recent H I surveys. This demonstrates that our estimator does, at least in a statistical sense, properly reproduce the distribution of H I mass in the local Universe. We have also used the data to examine whether the stellar mass-metallicity relation of galaxies depends on gas content, and we found a systematic change in gas fraction along this relation. In addition, at fixed stellar mass, galaxies with higher metallicities tend to contain less gas.

Finally, we would like to discuss how this work could be improved in future. First, the calibration sample (Sample II) is taken from HyperLeda, which is an inhomogeneous collection of data from different observational programs, each with different selection effects. It is not clear to what extent our calibrating sample is fully representative of the local galaxy population. The fact that we do see some systematic bias as a function of concentration index, suggests that as the bulge component becomes more prominent, our estimator, which is motivated by the Kennicutt-Schmidt law for galactic disks, may become increasingly inaccurate. We intend to test this using the larger and deeper samples that will soon become available from surveys such as ALFALFA and The GALEX Arecibo SDSS Survey (GASS) (Catinella et al. 2008). Another problem is that our calibrating sample lies at very low redshifts, so that any quantity that is measured from the SDSS spectra, such as metallicity, is heavily weighted to the central regions of the galaxies. We have skirted around this problem by dividing the galaxy population into two metallicity bins containing equal number of galaxies and carrying out a *relative comparison* between the gas fractions of the high and low-metallicity sub-samples at fixed stellar mass. This means that aperture bias are at least roughly the same for our two sub-samples. Nevertheless, it should be borne in mind that when we refer to metallicity in this paper, we are not talking about a global-average quantity.

We believe that it will be most interesting to apply our new indicators to galaxy samples where there is little prospect getting real H I mass measurements in the foreseeable future, for example at high redshift. The indicator may also be useful for applications where one would like to have some rough estimate of the cold gas available to fuel star formation, for example in satellite galaxies that are destined to merge with their parent object on some short timescale. We will be looking into such applications in our future work.

ACKNOWLEDGMENTS

WZ thanks MPA for invitation and hospitality. We thank the anonymous referee for helpful comments. This work has been supported by the Chinese National Natural Science

Foundation grants 10573020, 10603006, 10633020, 10803007, 10873016 and by National Basic Research Program of China (973 Program) 2007CB815403. This work has also been supported by the Young Researcher Grant of National Astronomical Observatories, Chinese Academy of Sciences, and the Max-Planck Society.

Funding for the SDSS and SDSS-II has been provided by the Alfred P. Sloan Foundation, the Participating Institutions, the National Science Foundation, the U.S. Department of Energy, the National Aeronautics and Space Administration, the Japanese Monbukagakusho, the Max Planck Society, and the Higher Education Funding Council for England. The SDSS Web Site is <http://www.sdss.org/>.

The SDSS is managed by the Astrophysical Research Consortium for the Participating Institutions. The Participating Institutions are the American Museum of Natural History, Astrophysical Institute Potsdam, University of Basel, University of Cambridge, Case Western Reserve University, University of Chicago, Drexel University, Fermilab, the Institute for Advanced Study, the Japan Participation Group, Johns Hopkins University, the Joint Institute for Nuclear Astrophysics, the Kavli Institute for Particle Astrophysics and Cosmology, the Korean Scientist Group, the Chinese Academy of Sciences (LAMOST), Los Alamos National Laboratory, the Max-Planck-Institute for Astronomy (MPIA), the Max-Planck-Institute for Astrophysics (MPA), New Mexico State University, Ohio State University, University of Pittsburgh, University of Portsmouth, Princeton University, the United States Naval Observatory, and the University of Washington.

REFERENCES

- Adelman-McCarthy J. K., Agüeros M. A., Allam S. S., Anderson K. S. J., Anderson S. F., Annis J., Bahcall N. A., Baldry I. K., et al., 2006, *ApJS*, 162, 38
- Ball N. M., Loveday J., Fukugita M., Nakamura O., Okamura S., Brinkmann J., Brunner R. J., 2004, *MNRAS*, 348, 1038
- Barrow J. D., Bhavsar S. P., Sonoda D. H., 1984, *MNRAS*, 210, 19P
- Bell E. F., McIntosh D. H., Katz N., Weinberg M. D., 2003, *ApJS*, 149, 289
- Blanton M. R., Brinkmann J., Csabai I., Doi M., Eisenstein D., Fukugita M., Gunn J. E., Hogg D. W., et al., 2003, *AJ*, 125, 2348
- Blanton M. R., Roweis S., 2007, *AJ*, 133, 734
- Blanton M. R., Schlegel D. J., Strauss M. A., Brinkmann J., Finkbeiner D., Fukugita M., Gunn J. E., Hogg D. W., et al., 2005, *AJ*, 129, 2562
- Boselli A., Lequeux J., Gavazzi G., 2002, *A&A*, 384, 33
- Bouché N., Cresci G., Davies R., Eisenhauer F., Förster Schreiber N. M., Genzel R., Gillessen S., Lehnert M., et al., 2007, *ApJ*, 671, 303
- Brinchmann J., Charlot S., White S. D. M., Tremonti C., Kauffmann G., Heckman T., Brinkmann J., 2004, *MNRAS*, 351, 1151
- Catinella B., Schiminovich D., Kauffmann G., 2008, in *American Institute of Physics Conference Series*, Vol. 1035, *The Evolution of Galaxies Through the Neutral Hydrogen Window*, Minchin R., Momjian E., eds., AIP, New York, pp. 252–255
- Cooper M. C., Tremonti C. A., Newman J. A., Zabludoff A. I., 2008, *MNRAS*, 390, 245
- De Lucia G., Blaizot J., 2007, *MNRAS*, 375, 2
- De Lucia G., Kauffmann G., White S. D. M., 2004, *MNRAS*, 349, 1101
- de Rossi M. E., Tissera P. B., De Lucia G., Kauffmann G., 2009, *MNRAS*, 395, 210
- de Vaucouleurs G., de Vaucouleurs A., Corwin Jr. H. G., Buta R. J., Paturel G., Fouque P., 1991, *Third Reference Catalogue of Bright Galaxies. Volume 1-3, XII*, 2069, Springer-Verlag, Berlin, Heidelberg, New York
- Ellison S. L., Patton D. R., Simard L., McConnachie A. W., 2008, *ApJL*, 672, L107
- Ellison S. L., Simard L., Cowan N. B., Baldry I. K., Patton D. R., McConnachie A. W., 2009, *MNRAS*, 396, 1257
- Erb D. K., Shapley A. E., Pettini M., Steidel C. C., Reddy N. A., Adelberger K. L., 2006, *ApJ*, 644, 813
- Fukugita M., Nakamura O., Okamura S., Yasuda N., Barntine J. C., Brinkmann J., Gunn J. E., Harvanek M., et al., 2007, *AJ*, 134, 579
- Gadotti D. A., 2009, *MNRAS*, 393, 1531
- Garnett D. R., 2002, *ApJ*, 581, 1019
- Giovanelli R., Haynes M. P., Kent B. R., Perillat P., Sainlonge A., Brosch N., Catinella B., Hoffman G. L., et al., 2005, *AJ*, 130, 2598
- Henning P. A., Staveley-Smith L., Ekers R. D., Green A. J., Haynes R. F., Juraszek S., Kesteven M. J., Koribalski B., et al., 2000, *AJ*, 119, 2686
- Hoopes C. G., Heckman T. M., Salim S., Seibert M., Tremonti C. A., Schiminovich D., Rich R. M., Martin D. C., et al., 2007, *ApJS*, 173, 441
- Jarrett T. H., Chester T., Cutri R., Schneider S., Skrutskie M., Huchra J. P., 2000, *AJ*, 119, 2498
- Kannappan S. J., 2004, *ApJL*, 611, L89
- Kauffmann G., Heckman T. M., White S. D. M., Charlot S., Tremonti C., Brinchmann J., Bruzual G., Peng E. W., et al., 2003, *MNRAS*, 341, 33
- Kennicutt Jr. R. C., 1998, *ApJ*, 498, 541
- Komatsu E., Dunkley J., Nolte M. R., Bennett C. L., Gold B., Hinshaw G., Jarosik N., Larson D., et al., 2009, *ApJS*, 180, 330
- Köppen J., Weidner C., Kroupa P., 2007, *MNRAS*, 375, 673
- Krumholz M. R., McKee C. F., Tumlinson J., 2008, *ApJ*, 689, 865
- Larson R. B., 1974, *MNRAS*, 169, 229
- Lequeux J., Peimbert M., Rayo J. F., Serrano A., Torres-Peimbert S., 1979, *A&A*, 80, 155
- Li C., White S. D. M., 2009, *MNRAS*, accepted, [arXiv:0901.0706](https://arxiv.org/abs/0901.0706)
- Michel-Dansac L., Lambas D. G., Alonso M. S., Tissera P., 2008, *MNRAS*, 386, L82
- Paturel G., Theureau G., Bottinelli L., Gougouenheim L., Coudreau-Durand N., Hallet N., Petit C., 2003, *A&A*, 412, 57
- Rosenberg J. L., Schneider S. E., 2002, *ApJ*, 567, 247
- Schmidt M., 1963, *ApJ*, 137, 758
- Springob C. M., Haynes M. P., Giovanelli R., 2005, *ApJ*, 621, 215
- Tremonti C. A., Heckman T. M., Kauffmann G., Brinch-

mann J., Charlot S., White S. D. M., Seibert M., Peng
E. W., et al., 2004, ApJ, 613, 898
Zwaan M. A., Briggs F. H., Sprayberry D., Sorar E., 1997,
ApJ, 490, 173
Zwaan M. A., Meyer M. J., Staveley-Smith L., Webster
R. L., 2005, MNRAS, 359, L30
Zwaan M. A., Staveley-Smith L., Koribalski B. S., Henning
P. A., Kilborn V. A., Ryder S. D., Barnes D. G., Bhathal
R., et al., 2003, AJ, 125, 2842

This paper has been typeset from a $\mathrm{T}_{\mathrm{E}}\mathrm{X}$ / $\mathrm{L}^{\mathrm{A}}\mathrm{T}_{\mathrm{E}}\mathrm{X}$ file prepared
by the author.